Crystal structure of a crustacean prophenoloxidase provides a clue to understanding the functionality of the type 3 copper proteins

Taro Masuda[1,*], Kyosuke Momoji[2], Takashi Hirata[2,4], and Bunzo Mikami[3]

[1] Laboratory of Food Quality Design and Development, Division of Agronomy and Horticultural Science, Graduate School of Agriculture, Kyoto University, Gokasho, Uji, Kyoto 611-0011, Japan

[2] Laboratory of Marine Bioproducts Technology, Division of Applied Biosciences, Graduate School of Agriculture, Kyoto University, Kitashirakawa-oiwakecho, Sakyo, Kyoto 606-8502, Japan

[3] Laboratory of Applied Structural Biology, Division of Applied Life Sciences, Graduate School of Agriculture, Kyoto University, Gokasho, Uji, Kyoto 611-0011, Japan

[4] Present address
Shijonawate Gakuen University Faculty of Rehabilitation
11-10, Hojo-5, Daito, Osaka 5740011 Japan

[*] Corresponding author:

Taro Masuda, Laboratory of Food Quality Design and Development, Division of Agronomy and Horticultural Science, Graduate School of Agriculture, Kyoto University, Tel.: +81 774 38 3765, Fax: +81 774 38 3765; E-mail: masutaro@kais.kyoto-u.ac.jp

Running title: Crystal structure of hexameric phenoloxidase

Abbreviations: PO, phenoloxidase; Hc, hemocyanin; NAG, N-acetylglucosamine; SAD, single-wavelength anomalous dispersion; L-DOPA, 3-(3',4'-dihydroxyphenyl)-L-alanine

Enzymes: Phenoloxidase **(E.C. 1.14.18.1)**

Database: Structural data are available in RSCB protein data bank under the accession number **3WKY.**

Keywords: phenoloxidase, tyrosinase, type 3 copper protein, hemocyanin, arthropod

Abstract

Phenoloxidase (PO), which is classified as a type 3 copper protein, catalyzes the hydroxylation of monophenol to *o*-diphenol and subsequent oxidation to the corresponding *o*-quinone. The geometry and coordination environment of the active site of the arthropod PO is very similar to that of the arthropod hemocyanin (Hc). However, unlike the POs, Hc is an oxygen carrier in crustaceans, and does not possess the PO activity in general. Recently, we identified a new type of proPO from a crustacean and designated it as proPOβ. This enzyme has many characteristics rather similar to Hc, such as its maturation, localization and oligomeric state. Here, we determined the crystal structure of proPOβ prepared from the hemolymph of kuruma prawns (*Marsupenaeus japonicus*) at 1.8 Å resolution. *M. japonicus* proPOβ forms a homo-hexamer rather similar to arthropod Hc. The geometry of the active copper site in proPOβ was nearly identical to that of arthropod Hc. Furthermore, the well characterized 'place holder' phenylalanine was observed (Phe72). However, the accessibility to the active site differed in several ways. First, another phenylalanine residue which shields the active site by interacting with a copper-coordinated histidine in crustacean Hc was substituted by valine in proPOβ structure. Second, two tyrosine residues, Tyr208 and Tyr209, both of which are absent in Hc, show the alternative conformations and form a pathway accessible to the reaction center. Thus, the present crystal structure clarified the similarities and differences in the activity of two closely related proteins, PO and Hc.

Introduction

Type 3 copper proteins are characterized by a coupled binuclear copper active site, in which each copper atom is coordinated by three ε-nitrogens of histidine residues [1]. In general, proteins in this class can incorporate a dioxygen reversibly between two coppers in a symmetric side on fashion that is required for the expression of their activities. Phenoloxidases (PO) or tyrosinase, which is a member of the type 3 copper proteins, catalyzes the hydroxylation of monophenol compounds to *ortho*-diphenol (mono-phenoloxidase activity) and subsequent oxidation to produce the corresponding *o*-quinone (*o*-diphenoloxidase activity). In contrast, a type 3 dicopper site containing members of a protein family called catechol oxidase catalyzes only the latter di-phenoloxidase reaction [2, 3]. PO is an indispensable component for innate immunity in arthropods [4]. However, its enzymatic activity should be strictly regulated, because PO generates reactive quinone species and triggers melanin formation. Accordingly, this class of enzyme is synthesized as a pro-form or inactive form, whose di-copper active center is shielded by itself or another protein. In general, arthropod PO is synthesized in hemocytes as an inactive pro-enzyme. It has been suggested that the activation of proPO requires several components [5]. One of the essential factors for this process is a clip domain serine protease variously called the prophenoloxidase activating protein (PAP), prophenoloxidase activating enzyme (PPAE) or prophenoloxidase activating factor (PPAF), which cleaves the propeptide of proPO [6-8]. This type of protease has a sequence homologous to the “easter” protease of drosophila, which is essential for pattern formation during embryonic development of drosophila [8-10]. In addition, several other factors, including serine protease homologues (SPHs), are also required for this activation process [11-13].

From the structural point of view, arthropod PO has a three-domain architecture resembling arthropod hemocyanin (Hc), another member of the type 3 copper proteins [14, 15]. In contrast to phenoloxidase, Hc lacks mono- or di-phenoloxidase activity under physiological conditions, but functions as an oxygen transport protein in mollusks and some arthropods, including crustaceans [16,

17]. One very intriguing phenomenon in regard to these two proteins is that PO oxidizes the mono- or di-phenol to the corresponding quinone, whereas Hc can only bind and transport molecular oxygen, although the two possess nearly identical active sites. In the last two decades, it has been suggested that arthropod or molluscan Hc will exhibit the *o*-diphenoloxidase activity under certain conditions which render the active site of Hc accessible to solvent and substrate [18-23].

Recently, the three-dimensional structures of a phenoloxidase from an insect [24] and tyrosinases from bacteria and fungi have been solved [25-28], and have revealed both the precise three-dimensional structures of the active site and the overall structure. Surprisingly, the structures of the di-copper active sites are nearly identical—e.g., the distances between the two coppers and the geometry of coordinated histidine side chains are the same. The three-dimensional structure of tyrosinase from bacteria suggested that this enzyme is composed of a single globular domain, in which the four helix bundle harbors the di-copper active site [25, 27]. The fungal tyrosinase forms a tetramer composed of two H and two L subunits. In the structure of tetramer, the catalytically active H subunit has a compact architecture similar to bacterial tyrosinase [28]. On the other hand, the only available structure of arthropod prophenoloxidase (PPO) (PDB ID: **3HHS**) is composed of a pro-region and three domains [24]. Among the domains, the active site is present in the domain II, which forms a 4-helix bundle similar to the case of fungal and bacterial tyrosinases. Arthropod PO and Hc have similar three-domain architectures and similar active site structures (the main chain rmsd between **3HHS** and **1LLA** was calculated to be 1.24 Å), and accordingly, they are suggested to be derived from a common ancestral protein [15]. One of the major differences is the quaternary structure; that is, the former forms a hetero-dimer [24] and the latter forms a hexamer as a single structural unit [29-31].

Previously, we identified a new type of PO from kuruma prawn (*Marsupenaeus japonicus*) and designated it as POβ [32]. This protein has strong mono- and di-PO activity, and thus is clearly a member of the PO family. However, it also has some physiological and structural characteristics rather similar to crustacean Hc as follows. i) The biosynthesis and localization manner: the POβ and

crustacean Hc are synthesized in the hepatopancreas with the N-terminal signal peptide (SP) [33], and present in hemolymph plasma [32], while the well known arthropod PO is synthesized in hemocyte cells without the SP, and present in hemocytes [34, 35]. ii) The quaternary structure: the proPOβ forms a hexamer similar to the case of Hc, while the arthropod PO usually forms a dimer [14, 24, 34-36]. In this study, we solved the crystal structure of the hexameric POβ as a pro-enzyme prepared from the hemolymph of kuruma prawn at a resolution of 1.8 Å. This structural analysis provides clues to the mechanism underlying the gain or loss of PO activity in type 3 copper proteins.

Results

Model quality and overall structure of proPOβ

The structure of proPOβ from kuruma prawn was determined by the single wavelength anomalous dispersion (SAD) method using anomalous scattering of copper atoms in the active site. The final structure was refined to a resolution of 1.8 Å. The overall coordinate error of the final model, estimated from Luzzati plots, was 0.17 Å. Root mean square deviations (rmsd) of bond lengths and angles from the ideal values were calculated using the PHENIX program [37] and are listed in Table 1. These values are well within acceptable limits, indicating that all of the structures have tight stereochemical constraints. A Ramachandran plot of the final structure shows that 98.3% and 1.56% of all residues were in the most favorable and additional favorable regions, respectively. Only one residue (Phe686) was in the disallowed region of the plot. This residue is a component of the C-terminal small circular peptide (see below) and has unusual ϕ and ψ angles. Refinement statistics are shown in Table 1.

The final model contained two subunits in the asymmetric unit of the *H*3 space group (Fig. 1a, b). When the 22nd valine residue from the initiated methionine residue is defined as the first amino acid residue [33], the model of the monomer begins at 8 and ends at the C-terminal 687 of the proPOβ sequence (Fig. 2). Two copper atoms are present in the active site of each monomer (Fig. 1c). As

described in our previous report, proPOβ has some N-linked glycosylation sites [32], some of which appeared to have the electron densities of N-acetylglucosamines (Fig. 1d). The residues that appeared to be glycosylated were as follows, Asn317, Asn422, Asn427, Asn456, Asn470, and Asn550 of each subunit (Fig. 1c). The residues 1-7, 40-44, 558-564 and 600-613 were missing in the final model because of the disorder. The overall folding of the proPOβ subunit is similar to that of proPO from *M. sexta* [24] and arthropod Hcs [29-31]. The main chain rmsd of alignable regions between proPOβ and **1LLA** (Hc from *L. Polyphemus*), **1HC1** (Hc from European spiny lobster), and **3HHS** (prophenoloxidase 1 from *M. sexta*) was calculated to 1.29, 1.59 and 1.68 Å with 24.2, 20.7 and 20.8% sequence identity, respectively (Fig. 2). According to the previous domain definition of arthropod PPO [24], the monomer subunit of proPOβ can be divided into three domains plus pro-region and additional C-terminal domain, e.g., the pro-region (1-52), the domain I (53-165), domain II (166-411), domain III (412-671), and the C-terminal domain (672-687) (Fig. 1c, 2). The C-terminal domain, which formed a circular peptide via a disulfide bond between Cys682 and the C-terminal Cys687 (Fig.1e), is unique to the proPOβ. The pro-region consists of short helices and a flexible loop. Although the reported cleavage sequence of insect proPO (NRFG) [34, 35] is not present in the sequence, a putative cleavage site with similar sequence ($DR^{28}LG$) is seen in the pro-region of proPOβ (Fig. 1c, Fig. 2). The pro-region faces to the surface of the domain I, and some interaction between them are seen. For examples, Phe15 (pro-region) interacts with Pro132 and Tyr117 (Domain I) via apolar contacts, while Tyr19 (pro-region) associates with Asp140 (Domain I) via a hydrogen bond. Although the overall structures of proPOβ and *M.sexta* PPO are closely related, the pro-regions of them highly vary each other, except the N-terminal short helix and the following loop (Glu8-Ser21 of proPOβ and Phe5-Pro18 of *M. sexta* PPO) (Fig. 2). Domain I and II have high content of α-helix, while domain III consists of a twisted, 7-stranded, anti-parallel β-sheet. Domain II is a catalytic domain harboring the type 3 copper site (Fig. 1c, 2). There are two disulfide bonds observed in domain III of each monomer (Cys572/Cys619 and Cys682/Cys687). However, proPOβ lacks another disulfide

bond that is well-conserved between PO (Cys586/Cys630 in PPO of *M. sexta*) and Hc (Cys534/Cys576 in *L. polyphemus*). The disulfide bond of the former (Cys572/Cys619 of proPOβ) is strictly conserved among the proPOβ, insect proPO [24], and arthropod Hcs [30], whereas the latter (Cys682/Cys687) is unique to proPOβ. The Cys687 is the C-terminal residue, and the disulfide bond with Cys682 forms a small circular peptide that lies on the neighboring 3-fold symmetric subunit and interacts with it (Fig.1e).

Hexameric structure and inter-subunit interactions of proPOβ

The native proPOβ formed a hexamer composed of six identical subunits (Fig. 3a, b). As described above, arthropod Hc also forms hexamer (Fig. 3c, d). Furthermore, there are 2- and 3-fold symmetry axes in the hexamers of both proPOβ and Hc. However, the overall packing differs between the two (Fig. 3). An asymmetric unit of the *H*3 crystal of proPOβ contains a dimer. Each subunit in an asymmetric unit is characterized by a 2-fold non-crystallographic symmetry axis (Fig. 1a). Along the symmetry axis, the helical (Val294-Met299) and loop (Leu288-Tyr293) regions in domain II interact with each other. The most prominent interaction occurs via π-π stacking between the two side chains of Tyr293 from the 2-fold symmetrical subunits (Fig. 1b). The dimer in the asymmetric unit can be assembled to the hexamer by a 3-fold symmetry operation. Hence, the hexamer of proPOβ has a 3-fold symmetry axis in its center (Fig. 3b left). In this respect, the hexamer consists of two trimers, which associate with each other in a face-to-face manner with a gap of 15 degrees. There is a large pore along the 3-fold symmetry axis of the hexameric proPOβ (Fig. 3b). The diameter of the pore is approximately 12.1 Å at the narrowest point, which is formed by three side chains of Asn519 (Fig. 3b right). Therefore, solvent and inorganic ions can penetrate freely along the central pore.

Interaction between the pro-region and three-domain core

The average isotropic temperature factor of the pro-region, domains I, II, and III, and the C-terminal

domain of proPOβ were calculated to 46.9, 31.6, 20.7, 28.4 and 50.3 $Å^2$. The high B value in the C-terminal domain can be attributed to the long disordered loop between the end of the domain III and the C-terminal circular peptide. In fact, the average B factor of the circular region (Cys682-687) was calculated to 28.5 $Å^2$. Similarly, the pro-region also has high temperature factor. The pro-region can be further divided into two regions (pro-region_1 and pro-region_2) being separated by the putative processing site Arg28. The pro-region_1 is ranging from the N-terminal to Arg28, while the pro-region_2 ranging from Leu29 to Glu52 (Fig. 2). The average B-values of the pro-region_1 and pro-region_2 were calculated to be 41.4 and 53.5 $Å^2$, respectively. The pro-region_1 interacted with the domain I by forming a hydrogen bond at the side chain of Tyr19 and the side chain of Asp140. This hydrogen bond weakly fixes the pro-region_1 to the three-domain core region, while the amino acid residues around the N-terminal and putative processing site are more flexible. The putative processing site (Arg28) is positioned at the end of a short helix (Fig. 1c, 2). The accessible surface areas (ASA) of the Arg28 were calculated as 59.7 $Å^2$ (A chain) and 55.6 $Å^2$ (B chain), and the main chain and side chain of the Arg28 had high temperature factors of more than 50 $Å^2$. These values are sufficient to suggest the possibility that Arg28 is the processing site.

The pro-region_2 has a higher temperature factor than the pro-region_1. In addition, the pro-region_2 contains a flexible loop that is missing in the current coordinate file. From the beginning of the pro-region_2 (Leu29) to Val46, no hydrogen bonds or apolar contacts with the three-domain core were observed. Judging from these observations, the pro-region_2 will become a disordered N-terminus after the processing at Arg28.

Active site structure

The coupled binuclear copper site consists of two coppers, CuA and CuB. This site is present in the center of the 4-helix bundle of domain II (Fig. 1c). In the catalytic site, the distance between the two coppers is 3.6 Å. The UV/vis absorption spectrum shows apparent maximal absorbance at 340 nm (Fig. S1), which is an important characteristic of oxy form Hc, PO and tyrosinase [3, 38-40]. This maximal

absorbance was not increased by the addition of equivalent molar of hydrogen peroxide (Fig. S1). From these results, the status of di-copper active site was defined as oxy form, which is harboring two oxygen atoms between two coppers (Fig. 4a). The CuA is coordinated by the NEs of three histidines (His199, His203, and His226), while the coordination residues to CuB are His357, His361, and His397 (Fig. 4b). All of these coordinated ligand histidines are derived from the core 4-helix bundle of domain II. This coordination environment is similar to that of insect PO and Hc from crustaceans. In the structure of tyrosinase from *Streptomyces*, one coordinated histidine residue is derived from a flexible loop, resulting in its side chain flexibility and the instability of CuA [25]. In contrast, the side chain flexibility was not observed in the crystal structure of proPOβ. The covalent cysteine-histidine bond which is usually observed in the active site of eukaryotic tyrosinase or catechol oxidase [2, 28, 41, 42] was not present in the proPOβ structure.

The coordinated histidine residues are stabilized by side chains of three phenylalanine residues (Phe72, Phe222, and Phe393) (Fig. 4b). The Phe72 corresponds to the "place-holder" residue Phe49 of the *L. polyphemus* Hc structure. To compare the structure around the di-copper active site of proPOβ to that of crustacean Hc, the superimposed structure is shown in Fig. 4c. As shown in Fig. 4c, there is additional one phenylalanine residue, Phe371, designated as F3 in the figure, around the active site of crustacean (*P. interruptus*) Hc (see also Table 2). Phe371 of crustacean Hc interacts with CuA-liganded histidine residue (H_A2), while the corresponding residue of proPOβ is substituted by valine (Fig. 4c, Table 2). In the structure of proPOβ, a cavity is observed in the vicinity of the active site (Fig. 4d). A cavity is also observed in crustacean Hc (Fig. 4e). However, the cavity of crustacean Hc doesn't expand to the active site, because F3 (Phe371) side chain which interacts with CuA liganded histidine (H_A2) blocks the active site (Fig. 4e). The positions of other three phenylalanines (Phe72, Phe222, and Phe393 of proPOβ) which are designated as F1, F2, and F4, respectively, are highly conserved among arthropod proPO and Hc (Table 2, Fig. 5).

Accessibility to the di-copper active site

Since the ASA values of the six histidine residues (His199, His203, His226, His 357, His361 and His397) of the active site were calculated to be 0.70, 10.5, 3.40, 0.20, 0.10, and 1.00 $Å^2$, the di-copper active site and coordinated histidine residues are almost completely buried in the structure of proPOβ. However, a cleft leading from the outside to the active site is observed (Fig. 6a, b). The amino acid residues separating the active site cavity from the cleft are Tyr208 and Tyr209 (Fig. 6c). The side chains of Tyr208 and Tyr209, whose ASA are calculated to be 29.1 and 25.3 $Å^2$, respectively, face both the cleft and the active site cavity (Fig. 6c). The side chain of Tyr209 has two conformations, while that of Tyr208 is fixed by a hydrogen-bond with the main chain carbonyl oxygen of Ala71 (Fig. 6b). As shown in Fig. 4b, Phe72 (F1), which corresponds to the place-holder, interacts with the imidazole ring of copper-coordinated His361 (H_B2) via π-π stacking. Thereby, the forward part of the domain I, especially from the Phe69 to the place-holder F1 (Phe72), and the cleft-shielding tyrosines (Tyr208 and Tyr209) are critical for the accessibility to the active site.

Mono- and di-PO activities of proPOβ and Hc

Since the POβ is synthesized as an inactive pro-enzyme much as in the case of other arthropod prophenoloxidases, the enzymatic activity needs to be enhanced by treatment with detergents or proteinases in vitro [32]. When the pro-form of POβ was mixed with *o*-diphenol substrate (1 mM of DOPA) and a detergent (0.1% sodium dodecylsulfate, SDS) as an activator, the proPOβ showed significant di-PO activity, while a trace amount of dopachrome was produced without adding the SDS (Fig. 7a). Purified Hc showed no detectable di-PO activity (Fig. 7a). Similarly, when mono-phenol (1 mM tyramine) was used as a substrate, only SDS-treated proPOβ produced dopachrome actively (Fig. 7b). In contrast, SDS-treated Hc and non-treated proPOβ showed little or no mono-PO activity under this condition and time course (Fig. 7b). However, when the incubation time was extended to 24 hours, the non-treated proPOβ showed trace mono-PO activity, which generated a detectable amount of

dopachrome, whereas Hc gained no mono-PO activity in spite of the SDS-treatment (Fig. 7c). These results indicated that the activity center was not fully blocked and a small amount of monophenol substrate can access the di-copper center, even if proPOβ was not activated by the addition of SDS or propeptide cleavage. On the other hand, purified Hc from the hemolymph of kuruma prawn could not be activated to gain mono- or di-phenoloxidase activity under these experimental conditions, irrespective of whether SDS was added.

The activity staining for di-PO activity was performed using 7.5% SDS-containing polyacrylamide gel after non-reducing SDS-PAGE. The PO activity was detected in the band of the purified proPOβ, whereas it was not detected in that of the purified Hc (Fig. S2). The apparent molecular weight of the band of proPOβ detected by CBB and activity staining was much larger than the 250 kDa marker. Judging from these results, activated proPOβ maintained the native hexameric conformation after treatment with the sample buffer containing 2% SDS.

Discussion

Arthropod PO possesses a distinctive overall structure compared with the tyrosinases from bacteria, fungi and mammals. In fact, the three-domain architecture of the arthropod PO is more remindful of the Hc architecture. Hence, the high resolution crystallographic analysis of arthropod PO will provide clues to the reasons for the functional difference between these type 3 copper proteins. The present structure of proPOβ provides some specific structural features, e.g. hexameric quaternary structure and the C-terminal circular peptide linked via an intra-molecular disulfide bond (Fig. 1e). Since the cleft leading to the di-copper active site positions outside of the hexamer (Fig. 6d), this quaternary structure would not affect the phenoloxidase activity. In fact, this enzyme expresses the activity in its native hexameric form (Fig. S2). The C-terminal circular region associates with the surface of neighboring 3-fold symmetry mate in the hexameric structure (Fig. 1e). It is possible that this hexameric structure is stabilized by this association to some extent.

In general, three or four phenylalanine residues, here designated the residues at positions F1, F2, F3, and F4, stabilize the conformation of the copper site, and sometimes they block the copper site to prevent non-specific oxidation of phenolic compounds. In regard to this surrounding of the active site, the present crystal structure reveals a distinctive difference compared with that of the crustacean Hc. In the structure of Hc from the crustacean *P. interruptus*, the F3 position is occupied by phenylalanine (Phe371), whose side chain interacts with the imidazole ring of histidine in the H_A2 position via stable π-π stacking and seems to shield the access to the CuA and occupies the active site cavity (Fig. 4c, 4e). The bulky phenylalanine residue at the F3 position is highly conserved among crustacean Hc, whereas this part is substituted to a relatively small residue in the sequence of proPO and Hc of chelicerates; i.e., the F3 position of proPOβ, *M. sexta* PPO and *L. polyphemus* Hc is substituted by valine (Val384), glutamate (Glu395) and threonine (Thr351), respectively (Fig. 5). In contrast to the case of crustacean Hc, the F3 valine residue of proPOβ does not shield the di-copper site, especially in the CuA direction, that generates the active site cavity in the vicinity of the active site (Fig. 4d). In the case of *M. sexta* PPO, the substituted glutamate side chain is reported to be flexible, suggesting that the side chain does not occupy the active site cavity. Similarly, the F3 position of the chelicerate Hc is substituted to threonine (Thr351 in *L. polyphemus* HcII) (Fig. 5, Table 2). It has been suggested that the chelicerate Hc can acquire the PO activity by the treatment with SDS [20, 21]. However, one of these studies also pointed out that the crustacean-type Hc has only trace PO activity, even when activated [20]. In accordance with this observation, we failed to activate the Hc of kuruma prawn by SDS treatment (Fig. 7, S2). Thus, it is possible that the F3 site has a critical role in determining whether or not the Hc can be activated to acquire the PO function. Similar substitution was observed between bacterial tyrosinase from *Bacillus megaterium* (TyrBm, PDB ID: **3NM8**) [27] and catechol oxidase from sweet potato (PDB ID: **1BT1**) [2]. Sendovski M. et al. discussed that the CuA shielding phenylalanine of catechol oxidase is substituted to valine in tyrosinase, and this substitution enable the hydroxylation of monophenol in tyrosinase [27]. More recently, to validate this hypothesis, this valine residue in TyrBm

was substituted to phenylalanine (V218F) and the enzymatic activity of the resultant mutant was assayed [43]. However, the mono-PO activity was not abolished, but rather enhanced by the substitution. This unexpected result is attributed to the flexibility of introduced phenylalanine residue, whose side chain is flipped out of the active site [43]. In contrast, the corresponding phenylalanine side chain of catechol oxidase (Phe361 of **1BT1**) is fixed well and covers the active site. This observation further supports the significance of the aromatic side chain, which covers the CuA site by associating with the side chain of CuA liganded histidine residue. Until now, the Phe49 of Hc from *L. polyphemus* has been considered a place-holder residue that act as a barrier to prevent the phenolic compounds from accessing the Hc active site [2, 30]. However, the place-holder phenylalanine is present in PPO of *M. sexta* (Phe88) and proPOβ (Phe72), both of which can be converted easily to active PO by treatment with SDS. Therefore, the phenylalanine of the F3 position can be considered as another factor for determining the activity.

Under the experimental conditions without the activator SDS, the di-copper active site is not directly exposed to the solvent and has a rigid conformation. However, leaky PO activity was observed without any activator (Fig. 7). One of the candidates for the entrance to the active site is a paired tyrosine residues (Tyr208 and Tyr209), which separates the active site cavity from the cleft (Fig. 6c). Accordingly, it is possible that these residues have a role for controlling the activity of this enzyme. Judging from their position, Tyr208 can be considered as a main shield of the active site cavity. The side chain of it is well fixed by the hydrogen bond with the main chain oxygen of Ala71 in the proPOβ. In contrast, the side chain of Tyr209 doesn't form a typical interaction with others and has two side chain conformations. This flexibility may cause a partial disorder of the shield and the leaky enzymatic activity of proPOβ.

As described above, the hydrophobic residues (Phe69, Phe70, Ala71, Phe72 (the place holder) have at least two structural roles, i.e. as a place holder for the Cu_B site (Phe72) (Fig. 4b) and a buckle for the shielding tyrosines (Ala71) (Fig. 6b). Thus, in order to fully open the activity center, the hydrophobic

amino acid residues (Phe69-Phe72) should be removed. This process may be achieved by SDS treatment in vitro, while it should be achieved by processing and other physiological activations in vivo. Over the last two decades, many components responsible for the arthropod proPO activation have been identified, mainly in insects [5]. An indispensable factor for the activation is one of the proPO activating factors (PPAFs): PPAF-I, II, and III [7, 8, 11, 44]. PPAF-I and –III belong to the catalytic group of clip domain serine proteases (SPs), while PPAF-II belongs to the non-catalytic group of the clip domain SP (serine protease homolog (SPH)). Although the processing of proPO by the protease is required for the activation, proPO does not acquire the PO activity by this pro-peptide cleavage alone [11, 12, 44]. The present structure supports this fact, because Phe69, Phe70, Ala71, and Phe72 (place-holder) very stably interact with the region in the vicinity of the di-copper active site (Fig. 6b). It is possible that SPHs such as PPAF-II, another essential factor for the activation of proPO, play a role in removing the region containing the place-holder from the di-copper active site, which is also resulting in the removal of the shield tyrosines. This idea is supported by the fact that PPAF-II has a hydrophobic cleft in its clip domain for association with the hydrophobic region of proPO [45].

The present study demonstrated that the proPOs from crustaceans and insects have similar three-dimensional structures. Together with the fact that some orthologs of insect proPO-activating factors were identified in crustaceans [46, 47], this suggests that similar activation mechanisms may exist in crustaceans. However, in crustaceans, research on prophenoloxidase and its activation factors has been focused on well-known hemocyto-type proPOs. It would be of great interest to investigate whether the specific activation factors are present for proPOβ, and whether this hemolymph-type proPO also plays a significant role in the innate immunity of crustacean.

Materials and Methods

Protein preparation, crystallization, and data collection

The proPOβ and Hc were purified from the hemolymph of live kuruma prawns by hydrophobic,

anion exchange, and size exclusion chromatography. The detailed purification method for purifying this protein was described elsewhere [32]. The protein concentration was estimated by the absorbance at 280 nm from the amino acid composition [48].

Initial crystals of proPOβ were obtained by sparse matrix screening within two weeks at 20°C using the hanging drop vapor diffusion method with a Mosquito® crystallization robot. The optimized crystallization drops were prepared by mixing equal volumes of mother liquid composed of 1.1 M sodium malonate, 0.5% Jeffamine ED-2001 (Hampton Research, Aliso Viejo, CA, USA), 0.1 M HEPES-Na (pH 7.0) and protein solution containing 10 mg/ml of purified proPOβ. Rhombohedral crystals belonging to the space group of *R*3 appeared within two weeks at 20°C. Flash cooling was carried out in a nitrogen gas stream at 100 K after brief soaking of the crystals in the mother liquid containing 20% ethyleneglycol. X-ray diffraction data from the crystals were collected up to 1.8 Å resolution at 100 K at the SPring-8 beamlines BL38B1, BL41Xu and BL26B1. The diffraction data were processed using hexagonal crystal settings (space group *H*3, a=b=156.7 Å, c=283.5 Å, a=b=90°, c=120°) using an HKL2000 software package (HKL Research, Charlottesville, VA, USA) [49].

Structural determination and refinement

SAD phases to 2.5 Å were calculated with the applications Autosol [50] and Phaser [51, 52] using data collected at an x-ray wavelength (1.3770 Å) corresponding to the peak of the x-ray fluorescence spectrum of copper. The improvement of the initial phases and peptide fragment modeling were performed using RESOLVE [53] and Autobuild [54]. The initial model was visualized and rebuilt using COOT 0.7 [55] and further modified on sigma-weighted (2 $|F_o|-|F_c|$) and ($|F_o|-|F_c|$) electron density maps, then refined with REFMAC5 [56] from the CCP4i suit 1.4.4 [57]. After repeated model rebuilding and refinement, the final model was refined using PHENIX [58] at 1.8 Å resolution. During the refinement, the di-copper sites were refined using a model containing two coppers and a water molecule without any restrains. Since the active site was defined as an oxy form by the resulting electron density maps and spectrophotometric analysis, refinement was carried out using the model

containing two oxygen atoms between two coppers under the restraint with modified cif file of Cu_2O_2 (CUO.cif in CCP4i suit). Finally, R_{work} dropped to 0.175 for all 239,448 reflections, and R_{free} dropped to 0.196 for all 11,997 reflections. Figures 1, 3, 4, and 6 were produced by PyMOL (DeLano Scientific, San Carlos, CA, USA). The images of the electrostatic potential of the protein surface were generated using the APBS application [59, 60]. The accessible surface area of amino acid residues in proPOβ sequence were calculated with the "Accessible Surface Area" application in the CCP4i suite.

UV/vis absorption spectrophotometry

The UV/vis absorption spectra were recorded using Hitachi U-2001 spectrophotometer (Hitachi, Tokyo, Japan) with a quartz cuvette of 1 cm path length. The concentration of purified proPOβ was 12.5 μM dissolved in 20 mM TrisHCl buffer (pH 7.8) containing 0.15 M NaCl. The spectrum was obtained by scaning the absorbance from 500 to 250 nm. Then, 12.5 μM of hydrogen peroxide, which was equivalent to the concentration of the enzyme, was added for three times. After every step of addition of hydrogen peroxide, the spectrum was recorded.

Analysis of PO enzymatic activity

To determine the enzymatic properties of the proPOβ and Hc from kuruma prawns, the concentrations of the purified proteins were adjusted to 0.3 mg ml^{-1}. The volume of each assay system was 200 μl, which contained the substrate (1 mM of L-DOPA or 1 mM of tyramine) in 20 mM Tris-HCl pH 7.4, 0.15 M NaCl, and 0.05 % (w/v) of SDS. The reaction was initiated by adding the enzyme to the final concentration of 7.5 μg ml^{-1} to a preincubated substrate solution at 30°C. PO activity was determined for 60 min at 30°C by monitoring the formation of dopachrome at 490 nm using a microplate reader (Tecan, Männedorf, Switzerland). Data were collected from at least four independent experiments every 30 seconds.

Non-reduced SDS-PAGE was performed using 7.5% polyacrylamide gel containing 0.1% SDS. 5 μg of each purified sample (proPOβ and Hc) was prepared by mixing with sample buffer containing final concentrations of 62.5 mM TrisHCl (pH 6.8), 2% SDS and 10% glycerol. After electrophoresis, one

gel was stained by CBB R-250, and another was dipped in a buffer containing 0.1% SDS and 1 mM of L-DOPA as a substrate.

Accession numbers

Coordinates and structural factors of proPOβ have been deposited in Protein Data Bank with accession number **3WKY**.

Acknowledgements

We are grateful to Dr. Takehiko Tosha at RIKEN SPring-8 for his helpful input and support with the crystallization. The synchrotron radiation experiments were performed at beamlines BL41XU, BL38B1 and BL26B1 of SPring-8 with the approval of the Japan Synchrotron Radiation Research Institute (JASRI) (proposal number: 2012B1953, 2012B1553, 2012B6741, 2012B1539). This work was financially supported by a Grant-in-Aid for Challenging Exploratory Research (Grant number 24658287) from JSPS and by the Towa foundation for food research.

Author contribution

TM, TH, and BM planed experiments. TM and KM performed experiments. TM and BM analyzed data. TM wrote the paper.

References

1. Rosenzweig AC & Sazinsky MH (2006) Structural insights into dioxygen-activating copper enzymes. *Curr Opin Struct Biol* **16**, 729-735.
2. Klabunde T, Eicken C, Sacchettini JC & Krebs B (1998) Crystal structure of a plant catechol oxidase containing a dicopper center. *Nat Struct Biol* **5**, 1084-90.
3. Hakulinen N, Gasparetti C, Kaljunen H, Kruus K & Rouvinen J (2013) The crystal structure of an extracellular catechol oxidase from the ascomycete fungus *Aspergillus oryzae*. *J Biol Inorg Chem* **18**, 917-29.
4. Cerenius L, Lee BL & Soderhall K (2008) The proPO-system: pros and cons for its role in

invertebrate immunity. *Trends Immunol* **29**, 263-271.

5. Cerenius L, Kawabata S.-i., Lee BL, Nonaka M & Soderhall K (2010) Proteolytic cascades and their involvement in invertebrate immunity. *Trends Biochem Sci* **35**, 575-583.

6. Tang H, Kambris Z, Lemaitre B & Hashimoto C (2006) Two proteases defining a melanization cascade in the immune system of Drosophila. *J Biol Chem* **281**, 28097-28104.

7. Satoh D, Horii A, Ochiai M & Ashida M (1999) Prophenoloxidase-activating enzyme of the silkworm, *Bombyx mori*. Purification, characterization, and cDNA cloning. *J Biol Chem* **274**, 7441-53.

8. Jiang H, Wang Y & Kanost MR (1998) Pro-phenol oxidase activating proteinase from an insect, *Manduca sexta*: a bacteria-inducible protein similar to Drosophila easter. *Proc Natl Acad Sci U S A* **95**, 12220-5.

9. Chasan R & Anderson KV (1989) The role of easter, an apparent serine protease, in organizing the dorsal-ventral pattern of the Drosophila embryo. *Cell* **56**, 391-400.

10. Lee SY, Cho, MY, Hyun JH, Lee KM, Homma KI, Natori S, Kawabata SI, Iwanaga S & Lee BL (1998) Molecular cloning of cDNA for pro-phenol-oxidase-activating factor I, a serine protease is induced by lipopolysaccharide or 1,3-beta-glucan in coleopteran insect, *Holotrichia diomphalia* larvae. *Eur J Biochem* **257**, 615-21.

11. Kim MS, Baek MJ, Lee MH, Park JW, Lee SY, Soderhall K & Lee BL (2002) A new easter-type serine protease cleaves a masquerade-like protein during prophenoloxidase activation in *Holotrichia diomphalia* larvae, *J Biol Chem* **277**, 39999-40004.

12. Gupta S, Wang Y & Jiang HB (2005) *Manduca sexta* prophenoloxidase (proPO) activation requires proPO-activating proteinase (PAP) and serine proteinase homologs (SPHs) simultaneously. *Insect Biochem Mol Biol* **35**, 241-248.

13. Felfoldi G, Eleftherianos I, Ffrench-Constant RH & Venekei I (2011) A Serine Proteinase Homologue, SPH-3, Plays a Central Role in Insect Immunity. *J Immuno.* **186**, 4828-4834.

14. Fujimoto K, Okino N, Kawabata S, Iwanaga S & Ohnishi E (1995) Nucleotide sequence of the cDNA encoding the proenzyme of phenol oxidase A1 of *Drosophila melanogaster*. *Proc Natl Acad Sci U S A* **92**, 7769-73.

15. Burmester T & Scheller K (1996) Common origin of arthropod tyrosinase, arthropod hemocyanin, insect hexamerin, and dipteran arylphorin receptor. *J Mol Evol* **42**, 713-728.

16. van Holde KE & Miller KI (1995) Hemocyanins. *Adv Protein Chem* **47**, 1-81.

17. Jaenicke E, Decker H, Gebauer WA, Markl J & Burmester T (1999) Identification, structure, and properties of hemocyanins from diplopod myriapoda. *J Biol Chem* **274**, 29071-29074.

18. Zlateva , DiMuro P, Salvato B & Beltramini M (1996) The o-diphenol oxidase activity of arthropod hemocyanin. *FEBS Lett* **384**, 251-254.

19. Salvato B, Santamaria M, Beltramini M, Alzuet G & Casella L (1998) The enzymatic properties of *Octopus vulgaris* hemocyanin: o-diphenol oxidase activity. *Biochemistry* **37**, 14065-14077.

20. Decker H, Ryan M, Jaenicke E & Terwilliger N (2001) SDS-induced phenoloxidase activity of

hemocyanins from Limulus polyphemus, *Eurypelma californicum*, and *Cancer magister*. *J Biol Chem* **276**, 17796-17799.

21. Decker H & Rimke T (1998) Tarantula hemocyanin shows phenoloxidase activity. *J Biol Chem* **273**, 25889-25892.

22. Suzuki K, Shimokawa C, Morioka C & Itoh S (2008) Monooxygenase activity of *Octopus vulgaris* hemocyanin. *Biochemistry* **47**, 7108-7115.

23. Morioka C, Tachi Y, Suzuki S & Itoh S (2006) Significant enhancement of monooxygenase activity of oxygen carrier protein hemocyanin by urea. *J Am Chem Soc* **128**, 6788-6789.

24. Li YC, Wang Y, Jiang HB & Deng JP (2009) Crystal structure of *Manduca sexta* prophenoloxidase provides insights into the mechanism of type 3 copper enzymes. *Proc Natl Acad Sci USA* **106**, 17002-17006.

25. Matoba Y, Kumagai T, Yamamoto A, Yoshitsu H & Sugiyama M (2006) Crystallographic evidence that the dinuclear copper center of tyrosinase is flexible during catalysis. *J Biol Chem* **281**, 8981-8990.

26. Matoba Y, Bando N, Oda K, Noda M, Higashikawa F, Kumagai T & Sugiyama M (2011) A molecular mechanism for copper transportation to tyrosinase that is assisted by a metallochaperone, caddie protein. *J Biol Chem* **286**, 30219-30231.

27. Sendovski M, Kanteev M, Ben-Yosef VS, Adir N & Fishman A (2011) First structures of an active bacterial tyrosinase reveal copper plasticity. *J Mol Biol* **405**, 227-37.

28. Ismaya WT, Rozeboom HJ, Weijn A, Mes JJ, Fusetti F, Wichers HJ & Dijkstra BW (2011) Crystal structure of *Agaricus bisporus* mushroom tyrosinase: identity of the tetramer subunits and interaction with tropolone. *Biochemistry* **50**, 5477-86.

29. Volbeda A & Hol WG (1989) Crystal structure of hexameric haemocyanin from *Panulirus interruptus* refined at 3.2 A resolution. *J Mol Biol* **209**, 249-79.

30. Hazes B, Magnus KA, Bonaventura C, Bonaventura J, Dauter Z, Kalk KH & Hol WG (1993) Crystal structure of deoxygenated *Limulus polyphemus* subunit II hemocyanin at 2.18 A resolution: clues for a mechanism for allosteric regulation. *Protein Sci* **2**, 597-619.

31. Magnus KA, Hazes B, Ton-That H, Bonaventura C, Bonaventura J & Hol WG (1994) Crystallographic analysis of oxygenated and deoxygenated states of arthropod hemocyanin shows unusual differences. *Proteins* **19**, 302-9.

32. Masuda T, Otomo R, Kuyama H, Momoji K, Tonomoto M, Sakai S, Nishimura O, Sugawara T & Hirata T (2012) A novel type of prophenoloxidase from the kuruma prawn *Marsupenaeus japonicus* contributes to the melanization of plasma in crustaceans. *Fish Shellfish Immunol* **32**, 61-68.

33. Kuyama H, Masuda T, Nakajima C, Momoji K, Sugawara T, Nishimura O & Hirata T (2013) Mass spectrometry based N- and C-terminal sequence determination of a hepatopancreas-type prophenoloxidase from the kuruma prawn, *Marsupenaeus japonicus*. *Anal Bioanal Chem* **405**, 2333-40.

34. Aspán A, Huang TS, Cerenius L & Söderhäll K (1995) cDNA cloning of prophenoloxidase from the freshwater crayfish *Pacifastacus leniusculus* and its activation. *Proc Natl Acad Sci U S A* **92**, 939-43.

35. Kawabata T, Yasuhara Y, Ochiai M, Matsuura S & Ashida M (1995) Molecular cloning of insect pro-phenol oxidase: a copper-containing protein homologous to arthropod hemocyanin. *Proc Natl Acad Sci U S A.* **92**, 7774-8.

36. Hall M, Scott T, Sugumaran M, Söderhäll K & Law JH (1995) Proenzyme of *Manduca sexta* phenol oxidase: purification, activation, substrate specificity of the active enzyme, and molecular cloning. *Proc Natl Acad Sci U S A.* **92**, 7764-8.

37. Adams PD, Grosse-Kunstleve RW, Hung LW, Ioerger TR, McCoy AJ, Moriarty NW, Read RJ, Sacchettini JC, Sauter NK & Terwilliger TC (2002) PHENIX: building new software for automated crystallographic structure determination. *Acta Crystallogr D Biol Crystallogr* **58**, 1948-1954.

38. Solomon EI, Sundaram UM & Machonkin TE (1996) Multicopper Oxidases and Oxygenases. *Chem Rev* **96**, 2563-2606.

39. Fujied, N, Murata M, Yabuta S, Ikeda T, Shimokawa C, Nakamura Y, Hata Y & Itoh S (2012) Multifunctions of MelB, a fungal tyrosinase from *Aspergillus oryzae*. *Chembiochem* **13**, 193-201.

40. Ginsbach JW, Kieber-Emmons MT, Nomoto R, Noguchi A, Ohnishi Y & Solomon EI (2012) Structure/function correlations among coupled binuclear copper proteins through spectroscopic and reactivity studies of NspF. *Proc Natl Acad Sci U S A* **109**, 10793-7.

41. Fujieda N, Murata M, Yabuta S, Ikeda T, Shimokawa C, Nakamura Y, Hata Y & Itoh S (2013) Activation mechanism of melB tyrosinase from *Aspergillus oryzae* by acidic treatment. *J Biol Inorg Chem* **18**, 19-26.

42. Fujieda N, Yabuta S, Ikeda T, Oyama T, Muraki N, Kurisu G & Itoh S (2013) Crystal structures of copper-depleted and copper-bound fungal pro-tyrosinase: insights into endogenous cysteine-dependent copper incorporation. *J Biol Chem* **288**, 22128-40.

43. Goldfeder M, Kanteev M, Adir N & Fishman A (2013) Influencing the monophenolase/diphenolase activity ratio in tyrosinase. *Biochim Biophys Acta* **1834**, 629-33.

44. Kwon TH, Kim MS, Choi HW, Joo CH, Cho MY & Lee BL (2000) A masquerade-like serine proteinase homologue is necessary for phenoloxidase activity in the coleopteran insect, *Holotrichia diomphalia* larvae. *Eur J Biochem* **267**, 6188-96.

45. Piao S, Song YL, Kim JH, Park SY, Park JW, Lee BL, Oh BH & Ha NC (2005) Crystal structure of a clip-domain serine protease and functional roles of the clip domains. *EMBO J* **24**, 4404-14.

46. Charoensapsri W, Amparyup P, Hirono I, Aoki T & Tassanakajon A (2011) PmPPAE2, a new class of crustacean prophenoloxidase (proPO)-activating enzyme and its role in PO activation. *Dev Comp Immunol* **35**, 115-24.

47. Cui Z, Liu Y, Wu D, Luan W, Wang S, Li Q & Song C (2010) Molecular cloning and characterization of a serine proteinase homolog prophenoloxidase-activating factor in the swimming

crab *Portunus trituberculatus*. *Fish Shellfish Immunol* **29**, 679-86.

48. Pace CN, Vajdos F, Fee L, Grimsley G & Gray T (1995) How to measure and predict the molar absorption coefficient of a protein. *Protein Sci* **4**, 2411-23.

49. Otwinowski Z & Minor W (1997) Processing of X-ray diffraction data collected in oscillation mode. *Macromol Crystallogr, Pt A* **276**, 307-326.

50. Terwilliger TC, Adams PD, Read RJ, McCoy AJ, Moriarty NW, Grosse-Kunstleve RW, Afonine PV, Zwart PH & Hung LW (2009) Decision-making in structure solution using Bayesian estimates of map quality: the PHENIX AutoSol wizard. *Acta Crystallogr D Biol Crystallogr* **65**, 582-601.

51. McCoy AJ, Storoni LC & Read RJ (2004) Simple algorithm for a maximum-likelihood SAD function. *Acta Crystallogr D Biol Crystallogr* **60**, 1220-1228.

52. McCoy AJ, Grosse-Kunstleve RW, Adams PD, Winn MD, Storoni LC & Read RJ (2007) Phaser crystallographic software. *J Appl Crystallogr* **40**, 658-674.

53. Terwilliger TC (2002) Automated structure solution, density modification and model building. *Acta Crystallogr D Biol Crystallogr* **58**, 1937-1940.

54. Terwilliger TC, Grosse-Kunstleve RW, Afonine PV, Moriarty NW, Zwart PH, Hung LW, Read RJ & Adams PD (2008) Iterative model building, structure refinement and density modification with the PHENIX AutoBuild wizard. *Acta Crystallogr D Biol Crystallogr* **64**, 61-69.

55. Emsley P, Lohkamp B, Scott WG & Cowtan K (2010) Features and development of Coot. *Acta Crystallogr D Biol Crystallogr* **66**, 486-501.

56. Murshudov GN, Vagin AA & Dodson EJ (1997) Refinement of macromolecular structures by the maximum-likelihood method. *Acta Crystallogr D Biol Crystallogr* **53**, 240-255.

57. Potterton E, Briggs P, Turkenburg M & Dodson E (2003) A graphical user interface to the CCP4 program suite. *Acta Crystallogr D Biol Crystallogr* **59**, 1131-1137.

58. Adams PD, Afonine PV, Bunkoczi G, Chen VB, Echols N, Headd JJ, Hung L-W, Jain S, Kapral G. J., Kunstleve, R. W. G., McCoy, A. J., Moriarty, N. W., Oeffner, R. D., Read, R. J., Richardson, D. C, Richardson JS, Terwilliger TC & Zwart PH (2011) The Phenix software for automated determination of macromolecular structures. *Methods* **55**, 94-106.

59. Holst M & Saied F (1993) Multigrid solution of the Poisson-Boltzmann equation. *J Comput Chem* **14**, 105-113.

60. Holst MJ & Saied F (1995) Numerical-solution of the nonlinear Poisson-Boltzmann equation - Developing more robust and efficient method. *J Comput Chem* **16**, 337-364.

Supporting information

Fig. S1 The Uv/vis absorption spectra of proPOβ and H_2O_2-treated proPOβ.

Fig. S2 Non-reduced SDS-PAGE analysis of purified proPOβ and Hc.

Table 1 Data collection and refinement statistics for the crystals of proPOβ.

	SAD	
Data collection statistics		
Beamline	BL38B1	BL41Xu
Space group	*H*3	*H*3
Lattice parameter (Å)	a=b=156.0, c=283.7	a=b=156.7, c=283.5
Wavelength (Å)	1.3770	1.0000
Resolution (highest shell) (Å)[a]	50-2.51 (2.60-2.51)	50-1.80 (1.86-1.80)
No. of unique reflections[a]	176,001 (17,576)	239,565 (23,653)
Completeness (%)[a]	100 (100)	99.7 (98.4)
Data redundancy [a]	5.8 (5.5)	3.3 (3.0)
R_{merge} [b a]	0.064 (0.170)	0.052 (0.363)
$I/\sigma(I)$ [a]	24.2 (19.4)	11.9 (2.46)
Number of heavy atoms	4	
F.O.M. (Initial/Density modified)	0.39 / 0.72	
Refinement statistics		
Resolution (Å) [a]		34.8-1.80 (1.82-1.80)
Used reflections [a]		239,452 (7,204)
Residues in an asymmetric unit		1,310
Number of Copper atoms / water molecules		4/ 1,135
Number of NAG residues / Etyleneglycol		14/ 9
R/R_{free} [c a]		0.175 (0.260) / 0.196 (0.275)
Rms deviations from ideality		
Bond length (Å)		0.007
Bond angle (deg.)		1.108
Wilson B (Å^2)		20.01
Isotropic B factor (Å^2) Protein/ Cu_2O_2/ solvents		28.3/ 27.5/ 34.5

[a] Values in parentheses are for the highest resolution shell.

[b] $R_{merge}=\sum_{hkl}\sum_i|I_i(hkl)-\langle I(hkl)\rangle|/\sum_{hkl}\sum_i(hkl)$, where $I_i(hkl)$ is the integrated intensity of a reflection, and $\langle I(hkl)\rangle$ is the mean intensity of multiple corresponding symmetry-related reflections.

[c] $R/R_{free}=\sum_{hkl}||F_{obs}|-|F_{calc}||/\sum_{hkl}|F_{obs}|$, where R and R_{free} are calculated using the test reflections, respectively. The test reflections (5 %) were held aside and not used during the entire refinement process.

Figure legends

Figure 1

Three-dimensional structure of *M. japonicus* proPOβ. (PDB ID: **3WKY**)

(a) Two subunits in an asymmetric unit of the *H*3 crystal are viewed down a 2-fold non-crystallographic symmetry axis. (b) Interaction of two symmetry-related subunits via π-π stacking between two side chains of Tyr293 in proPOβ. (c) Domains of a proPOβ subunit are viewed from two angles. The pro-domain, domains I, II, and III, and C-terminal domain are colored red, green, yellow, magenta, and blue, respectively. The putative processing site (Arg28), glycosylated asparagine residues and added N-acetyl-D-glucosamine residues are shown as sticks. To show clearly the position of the di-copper active site in a subunit of proPOβ, amino acid residues around the site are shown as sticks. Two copper atoms are shown as red spheres. (d) The structure of a glycosylated asparagine residue (Asn456) and adducted NAG residues. The electron density of the 2 $|F_o|$-$|F_c|$ map for these residues is contoured at 1.5σ and shown in light blue mesh. (e) Structure of the circular region of the C-terminal domain and its interaction with the surface of the neighboring subunit (stereoview). Amino acid residues forming the circular peptide are shown as sticks and the main chain of the original subunit of this circular region is shown as an orange line. The electron density for the circular region is contoured at 1.2σ and shown in pink mesh. The surface of the neighboring subunit interacting with the circular peptide is depicted in grey.

Figure 2

Amino acid sequence alignment between the proPOβ and *M. sexta* PPO.

Defined Domains (Signal peptide, Pro-domain, Domain I, II, III, and C-terminal domain) are indicated by bars colored in grey, red, green, yellow, magenta, and blue. The signal peptide and the C-terminal domain are specifically present in proPOβ sequence. The α-helices and β-strands assigned by the DSSP (http://swift.cmbi.ru.nl/gv/dssp/) application are shown by blue columns and red arrowheads,

respectively. The deduced processing sites of proPOβ and *M. sexta* PPO are shown as black highlighted. The copper coordinated histidine residues are highlighted in red, while the residues surrounding the active site are highlighted in blue (see also Table 2). Identical and similar amino acid residues are indicated by * and :, respectively. GenBank accession numbers of kuruma prawn proPOβ and *M. sexta* are **AB617654** and **3HHS_A**.

Figure 3

Hexameric structure of proPOβ and Hc.

(a)(b) Hexameric structure of proPOβ viewed down a 2-fold (a) and 3-fold symmetry axis (b). The residues Asn519, which form the internal surface of the 3-fold symmetry channel, are depicted as sticks. The enlarged image around the 3-fold symmetry axis (the boxed region in the left panel) is shown in right panel. (c)(d) Hexameric structure of the crustacean Hc from *P. interruptus* (PDB ID: **1HCY**) viewed down a 2-fold (c) and 3-fold symmetry axis (d).

Figure 4

Three-dimensional structure of the type 3 copper site of proPOβ.

(a) The six copper-liganded histidines are shown as sticks. Two copper atoms are shown as red spheres, and the oxygen atoms between two coppers are shown as blue spheres. The electron density of the 2 $|F_o|$-$|F_c|$ map for the di-copper site is contoured at 2.0σ and shown in light blue mesh. (b) Structure around the di-copper site of proPOβ together with the associated phenylalanine residues. (c) Superimposed structures of the di-copper active site of the proPOβ (the present structure, PDB ID: **3WKY**) (red) and crustacean Hc (**1HC1**) (cyan) (stereoview). The CuA-liganded histidines are designated H_A1, H_A2, and H_A3. Similarly, the CuB-liganded histidines are designated H_B1, H_B2, and H_B3. Those residues in the vicinity of the liganded histidines are designated F1, F2, F3, and F4. The corresponding amino acid residues of the two members, proPOβ, and *P. interruptus* Hc, are shown in

Table 2. (d)(e) Detailed structure around the di-copper active sites of proPOβ (d) and crustacean Hc (e). The discussed amino acid residues are shown as sticks, while the copper atoms are as red spheres. The culled cavities and pockets are shown as brown blobs. The F3 residues, which are Val384 in proPOβ and Phe371 in crustacean Hc, are indicated by circles.

Figure 5

Partial amino acid sequence alignment of proPOs and Hcs from arthropods.

The amino acid sequences around the F3 position were aligned between the proPO and Hc of the following species. proPOβ: *M. japonicus* proPOβ, presented here; MsPO: chain A of *M. sexta* PPO (accession code: **3HHS_A**); MjPO: *M. japonicus* proPO (**BAB83773**); PmPO2: *Penaeus monodon* proPO2 (**ACJ31817**); LpHcIV, IIIb, IIIa, II, and VI: *L. polyphemus* Hc subunits (**CAJ91099**, **CCA94914**, **CAJ91098**, **CAJ91097** and **CAJ91100**, respectively); PmHc: *P. monodon* Hc (**AEB77775**); MjHcL and MjHcY: *M. joponicus* Hc L and Y subunits (**ABR14693** and **ABR14694**); LvHc: *Litopenaeus vannamei* Hc (**CAB85965**); PlHc: *Pacifastacus leniusculus* Hc (**AAM81357**).

Figure 6

Active site cleft and di-copper active site of proPOβ.

(a) The surface representation of a proPOβ monomer. The molecular surface of a proPOβ monomer is represented as gray. The copper coordinated histidine residues are shown as green sticks, while Tyr208 and Ty209 are as red sticks. The exposed surface area of the tyrosine residues are shown as red. (b) An expanded image of the active site cleft (stereoview). The red portion of the surface represents the exposed surfaces of Tyr208 and Tyr209. The copper coordinated histidine residues, the place-holder phenylalanine (Phe72) and its neighboring residues (Phe69, Phe70 and Ala71) of the domain I are also shown as sticks. (c) A summarized figure of the positional relations among the cleft, cavity, and the di-copper active site of proPOβ (stereoview). The surfaces of the cleft and cavity are shown as brown.

To simplify the figure, the Cu-liganded histidine residues of proPOβ are represented as H_A1, H_A2, H_A3, H_B1, H_B2 and H_B3. The definitions of these histidine residues are shown in Table 2. (d) The surface of proPOβ hexamer is represented as brown. The red portion is the surface of the active site cleft shown in Figure 6a and 6b.

Figure 7

Mono- and *o*-diphenoloxidase activity of proPOβ and Hc of *M. japonicas*

(a)(b) Progression plot of dopachrome formation monitored by the absorbance at 490 nm, when *o*-diphenol DOPA (a) and monophenol tyramine (b) were used as substrates. (c) An image of the microplate used in the mono-PO activity assay. After monitoring the absorbance at 490 nm, this plate was left in a dark room for 24 hrs at 25 °C. Under this condition, the proPOβ samples, which were not activated with SDS, also generated detectable dopachrome from monophenol substrate tyramine. Data are represented as mean +/- SD.

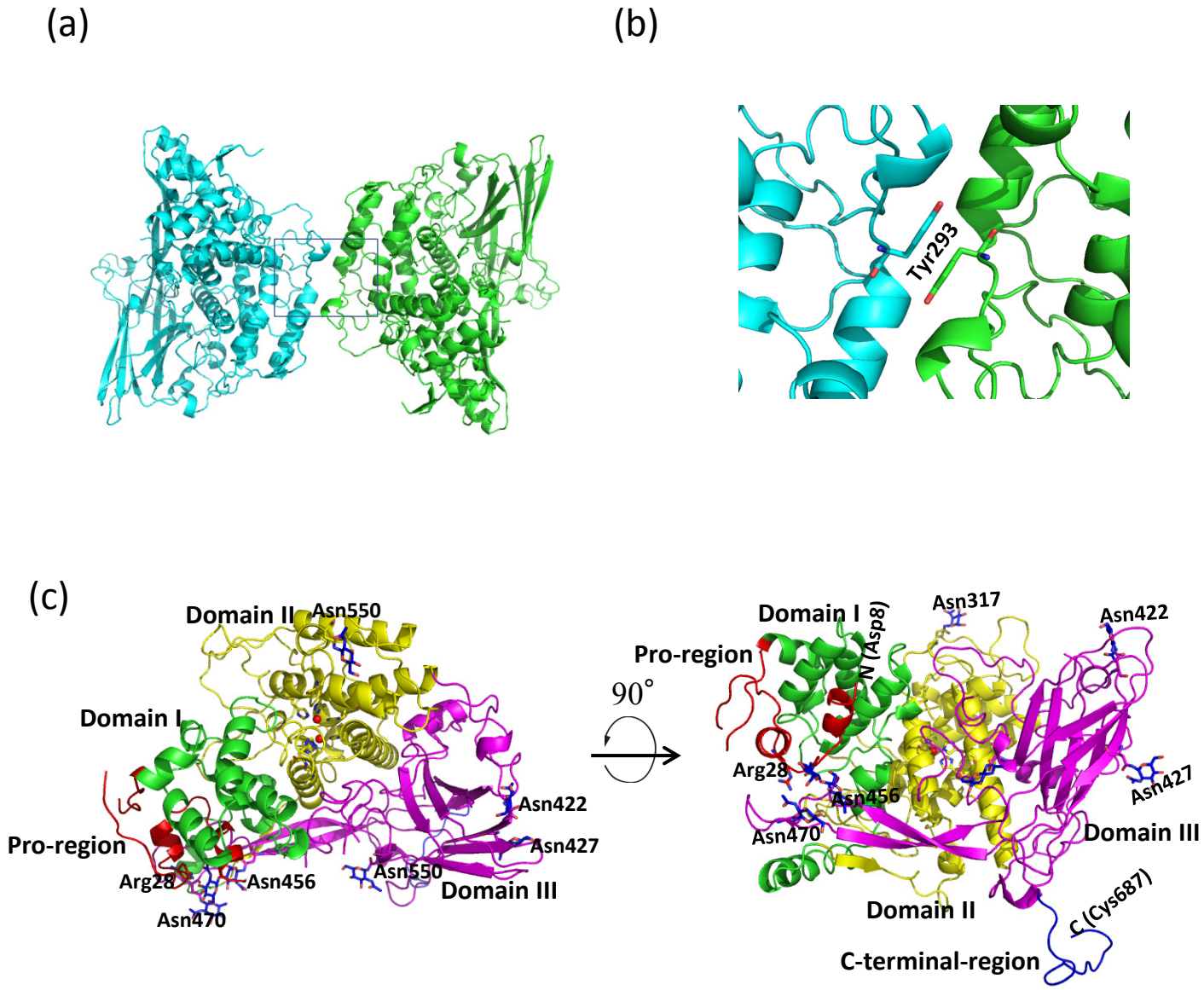
(a)
(b)
Tyr293
(c)
Domain II
Asn550
Domain I
Pro-region
Arg28
Asn456
Asn470
Asn422
Asn427
Asn550
Domain III
90°
Domain I
Asn317
Asn422
Pro-region
N (Asp8)
Arg28
Asn456
Asn470
Asn427
Domain III
Domain II
C (Cys687)
C-terminal-region

Figure 1

(d)

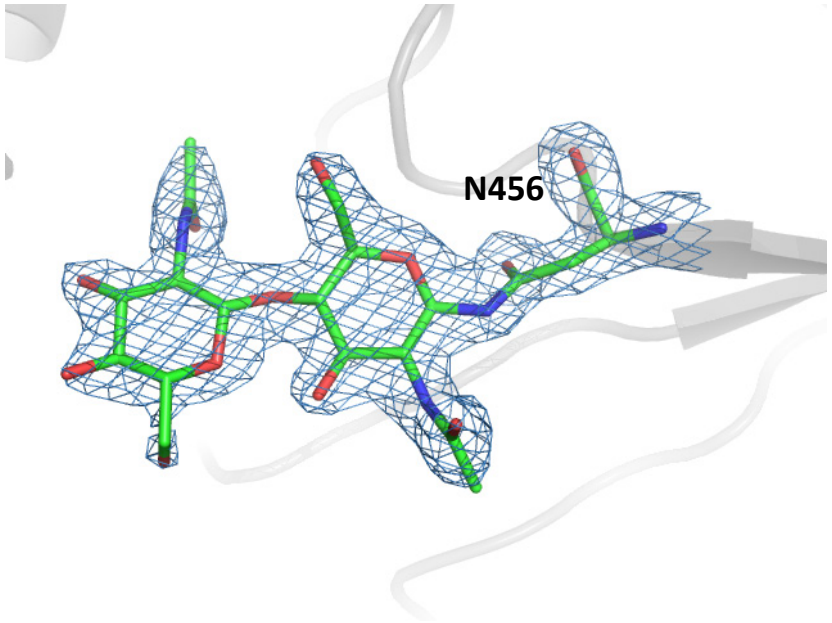

Figure 1 (continued)

(e)

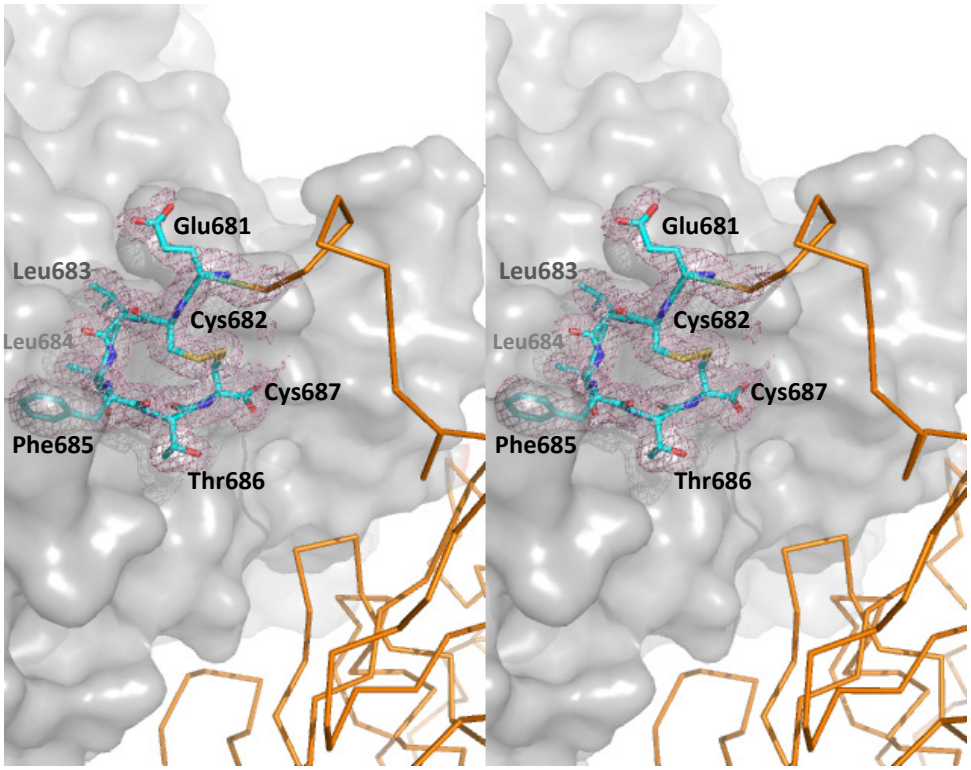

Figure 1 (continued)

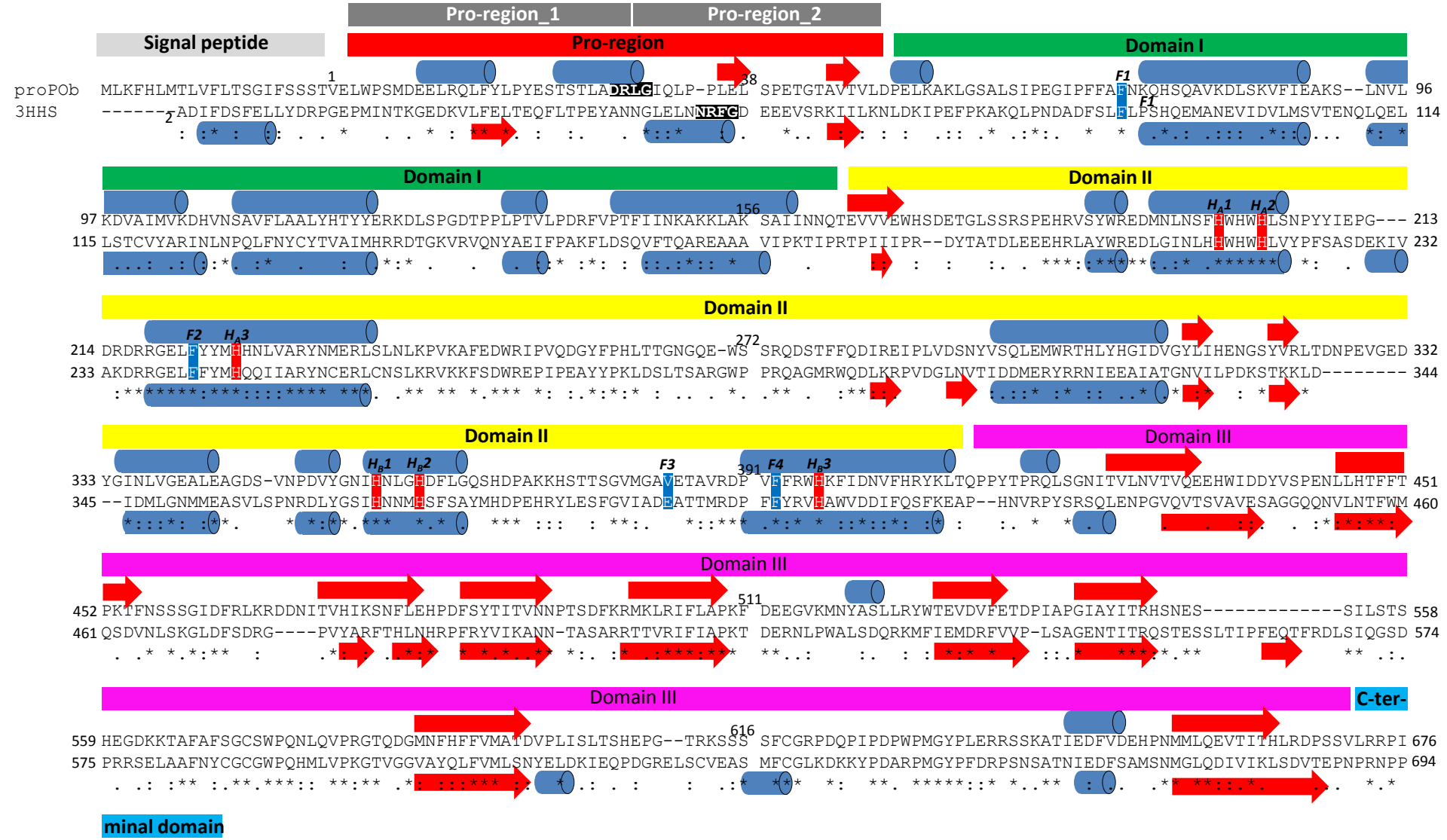
Pro-region_1
Pro-region_2
Signal peptide
Pro-region
Domain I
Domain II
Domain III
C-ter-
minal domain
proPOb
3HHS
F1
F2
F3
F4
H_A1
H_A2
H_A3
H_B1
H_B2
H_B3
677 SERKECLLFTC 687
695 A----------

Figure 2

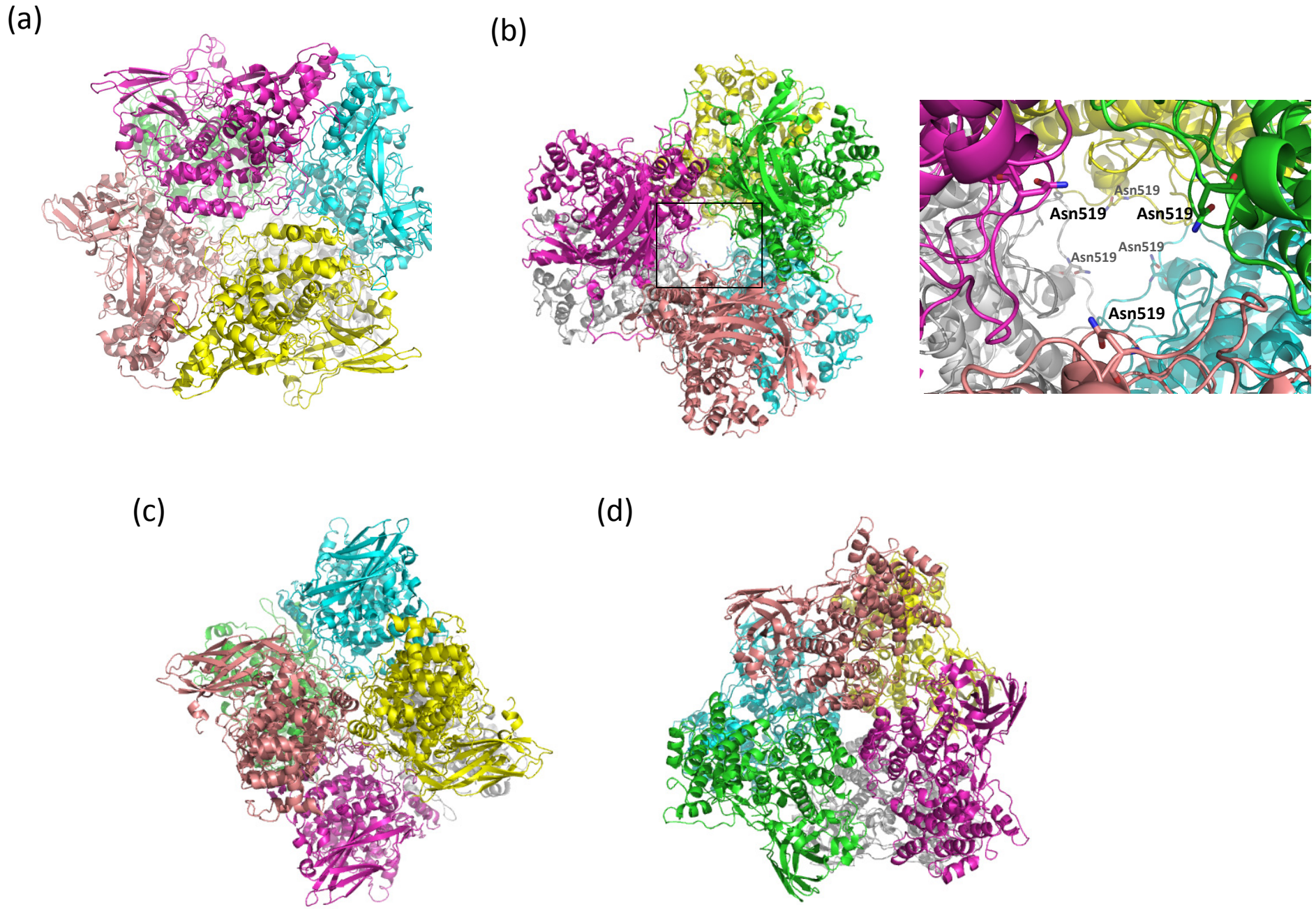

Figure 3

(a)

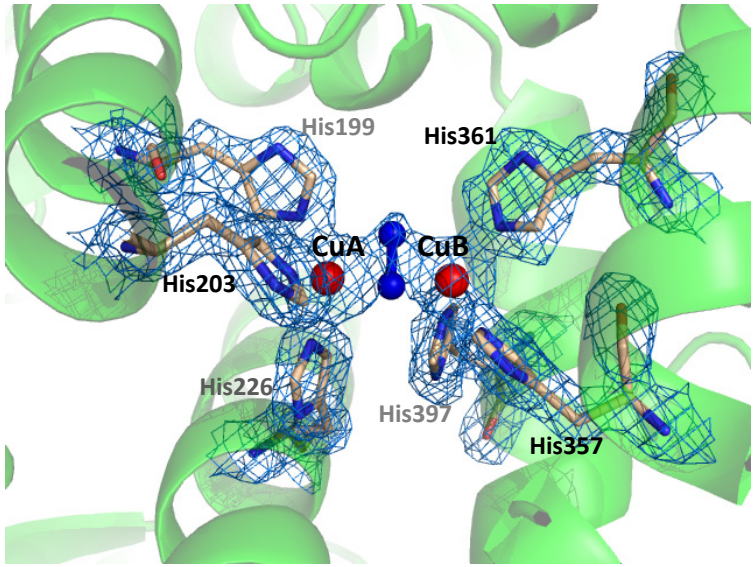
His199
His361
CuA
CuB
His203
His226
His397
His357

(b)

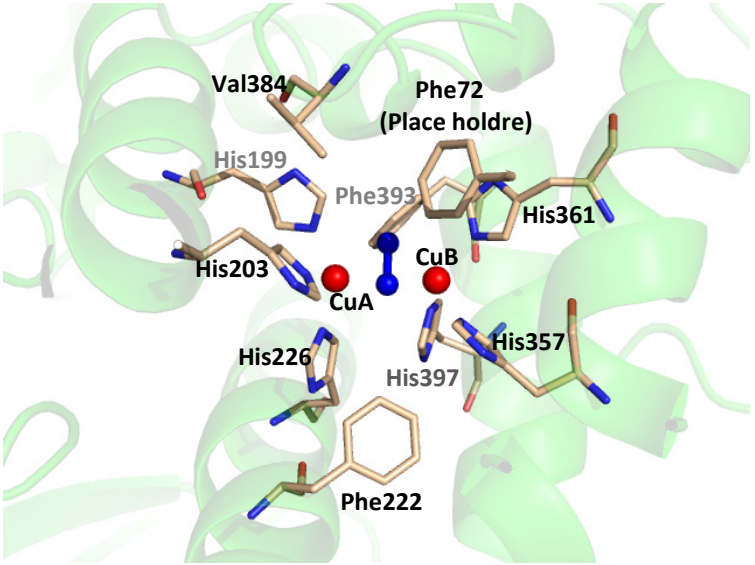
Val384
Phe72
(Place holdre)
His199
Phe393
His361
His203
CuB
CuA
His357
His226
His397
Phe222

(c)

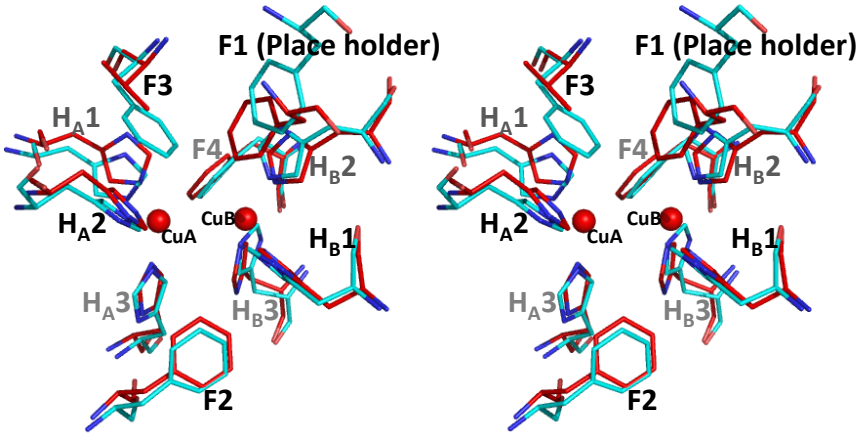
F1 (Place holder)
F3
H_A1
F4
H_B2
H_A2
CuA
CuB
H_B1
H_A3
H_B3
F2
F1 (Place holder)
F3
H_A1
F4
H_B2
H_A2
CuA
CuB
H_B1
H_A3
H_B3
F2

Figure 4

(d)

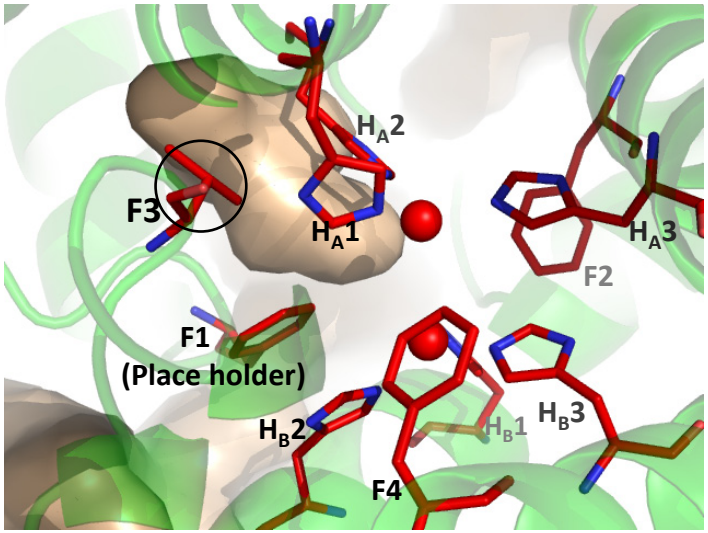

(e)

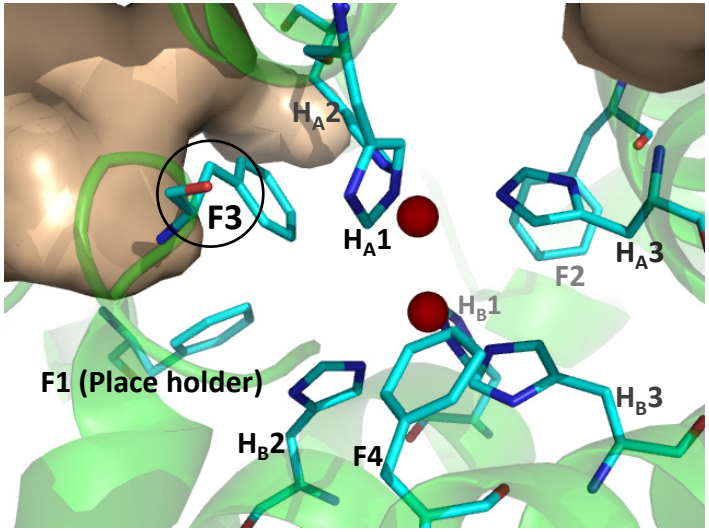

Figure 4 (continued)

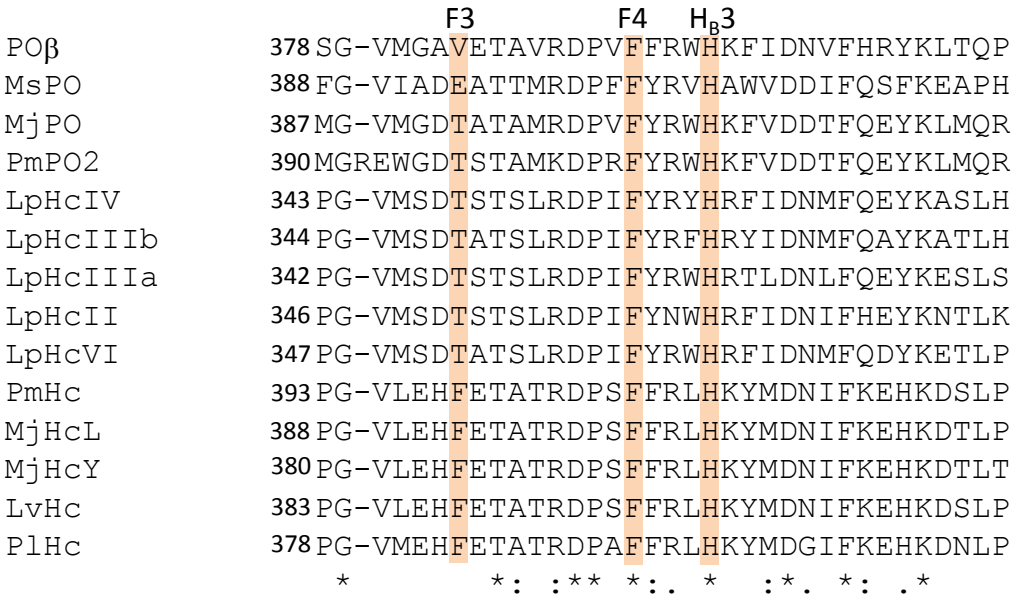
F3
F4
H_β3
POβ 378 SG-VMGAVETAVRDPVFFRWHKFIDNVFHRYKLTQP
MsPO 388 FG-VIADEATTMRDPFFYRVHAWVDDIFQSFKEAPH
MjPO 387 MG-VMGDTATAMRDPVFYRWHKFVDDTFQEYKLMQR
PmPO2 390 MGREWGDTSTAMKDPRFYRWHKFVDDTFQEYKLMQR
LpHcIV 343 PG-VMSDTSTSLRDPIFYRYHRFIDNMFQEYKASLH
LpHcIIIb 344 PG-VMSDTATSLRDPIFYRFHRYIDNMFQAYKATLH
LpHcIIIa 342 PG-VMSDTSTSLRDPIFYRWHRTLDNLFQEYKESLS
LpHcII 346 PG-VMSDTSTSLRDPIFYNWHRFIDNIFHEYKNTLK
LpHcVI 347 PG-VMSDTATSLRDPIFYRWHRFIDNMFQDYKETLP
PmHc 393 PG-VLEHFETATRDPSFFRLHKYMDNIFKEHKDSLP
MjHcL 388 PG-VLEHFETATRDPSFFRLHKYMDNIFKEHKDTLP
MjHcY 380 PG-VLEHFETATRDPSFFRLHKYMDNIFKEHKDTLT
LvHc 383 PG-VLEHFETATRDPSFFRLHKYMDNIFKEHKDSLP
PlHc 378 PG-VMEHFETATRDPAFFRLHKYMDGIFKEHKDNLP
* *: :** *:. * :*. *: .*

Figure 5

(a)

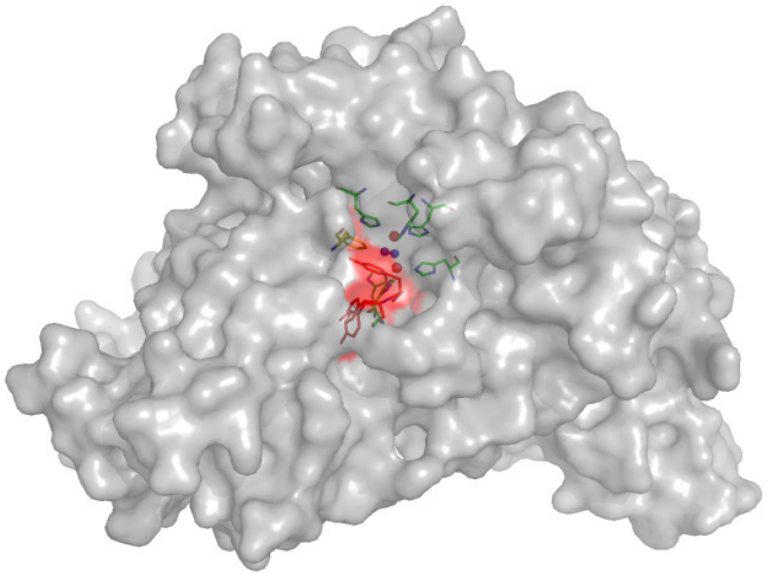

(b)

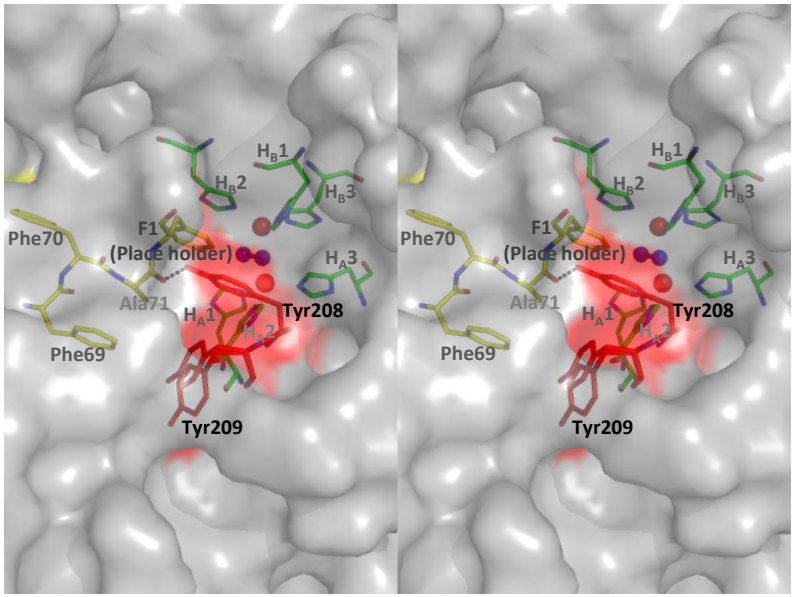

(c)

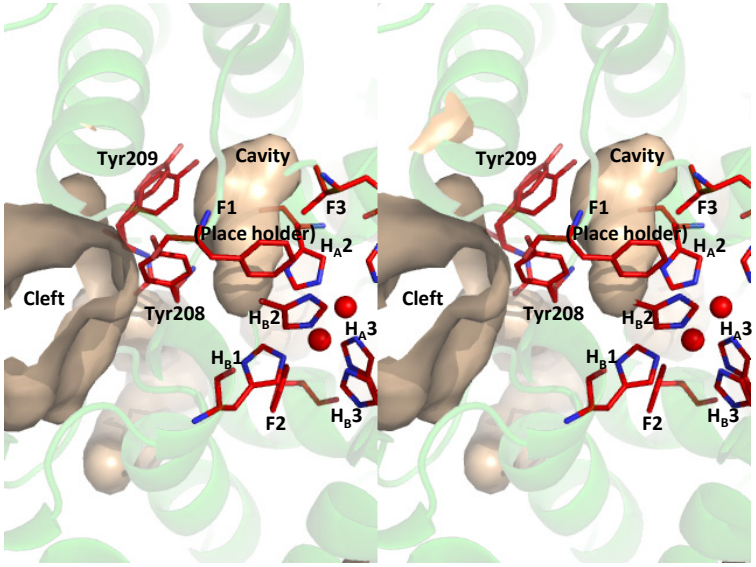

(d)

Figure 6

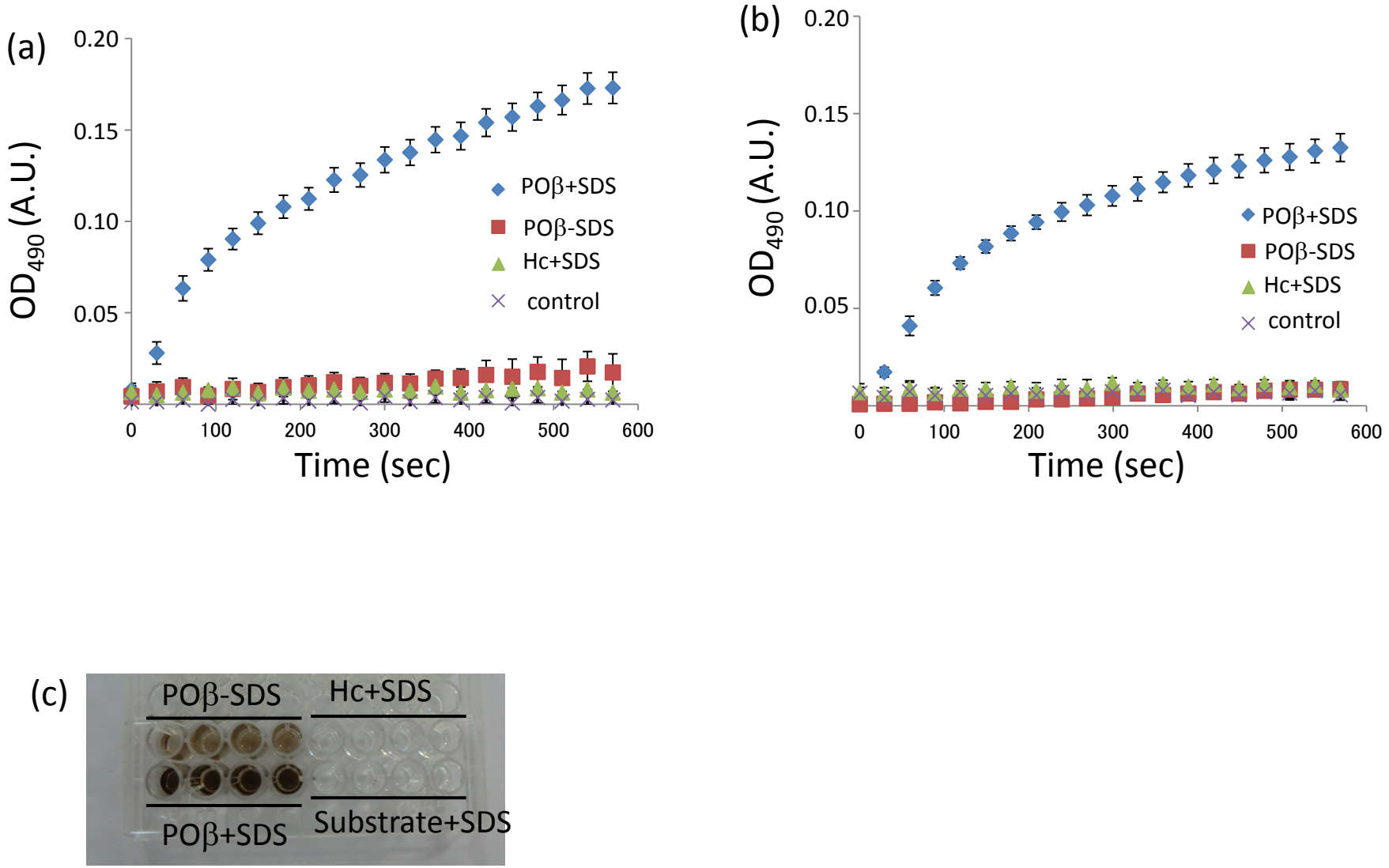
(a)
0.20
0.15
0.10
0.05
OD490 (A.U.)
POβ+SDS
POβ-SDS
Hc+SDS
control
0
100
200
300
400
500
600
Time (sec)
(b)
0.20
0.15
0.10
0.05
OD490 (A.U.)
POβ+SDS
POβ-SDS
Hc+SDS
control
0
100
200
300
400
500
600
Time (sec)
(c)
POβ-SDS
Hc+SDS
POβ+SDS
Substrate+SDS

Figure 7

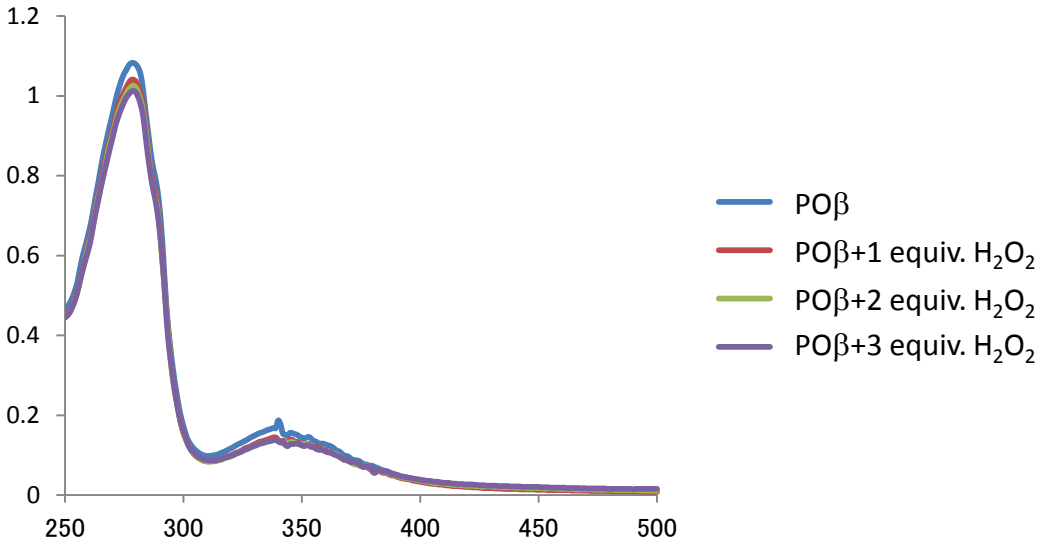

Figure S1

The Uv/vis absorption spectra of proPOβ and H_2O_2-treated proPOβ. The enzyme concentration was 12.5 mM, and 1, 2, 3 equivalent molar of H_2O_2 was added to the enzyme mixture.

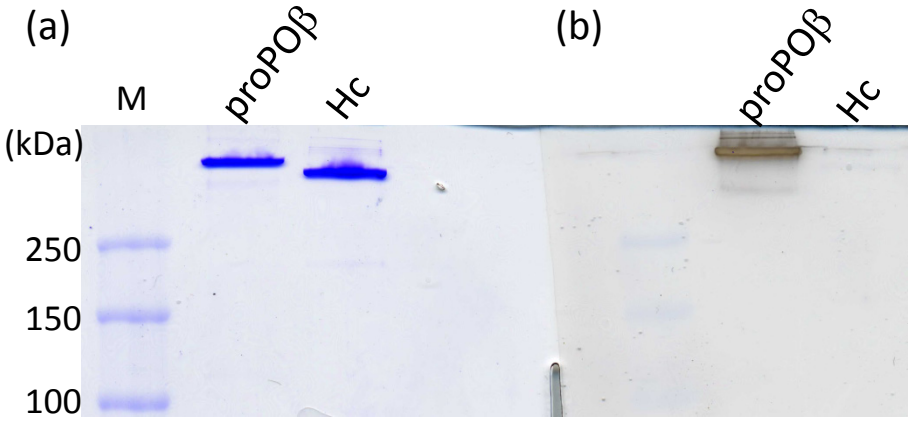

Non-reduced SDS-PAGE analysis of purified proPOβ and Hc. Purified proPOβ and Hc were separated by non-reduced SDS-PAGE, followed by the detection with CBB R250 staining (a) and activity staining using L-DOPA as a substrate (b).

Fig. S2